

NUMERICAL MODELING OF SURFACE ACOUSTIC WAVES FOR ELECTRONIC FILTER DESIGN

**Alonso Fernández García¹, Ericka Yatzil García Figueroa²,
Luis Alfonso Villa Vargas³, Juan Carlos Sánchez García¹,
Marco Antonio Ramírez-Salinas³,
Verónica Iraís Solís-Tinoco^{3,4*}, Miguel Ángel Alemán-Arce³**

¹Escuela Superior de Ingeniería Mecánica y Eléctrica, Instituto Politécnico Nacional, 04440, Ciudad de México, México.

²Unidad Profesional Interdisciplinaria en Ingeniería y Tecnologías Avanzadas UPIITA -IPN. Ingeniería Mecatrónica. Ciudad de México, 07340, México.

³Centro de Investigación en Computación del Instituto Politécnico Nacional, Laboratorio de Microtecnología y Sistemas Embebidos. Ciudad de México, 07738. México.

⁴Instituto de Ciencias Aplicadas y Tecnología, Universidad Nacional Autónoma de México, Ciudad de México, 04510, México.

*irais.solis@cic.ipn.mx

Abstract

Surface acoustic wave (SAW) filters are widely used in most of the electronic industry. In this work, a detailed methodology for the design and numerical simulation of a SAW bandpass filter in a 128° YX LiNbO_3 piezoelectric material is presented. The SAW filter operates using a delay line configuration. It consists of $N_p = 20$ double finger pairs, with a port separation of $l = 1293.6 \mu\text{m}$, an acoustic aperture of $W = 2597.32 \mu\text{m}$, a finger width of $r = 16.17 \mu\text{m}$, and a finger thickness of $h = 300 \text{ nm}$ with an acoustic wavelength of $\lambda = 129.36 \mu\text{m}$. The results showed an insertion loss level of $IL = -10.39 \text{ dB}$, side lobe levels of $SLL = -33.01 \text{ dB}$, and a null bandwidth value of $NBW = 3 \text{ MHz}$. The conductance calculations exhibited a maximum value of 83 mS , while the susceptance showed maximum and minimum values of 120 mS and 8 mS , respectively. This methodology is beneficial for enhancing the understanding of SAW filter design. Besides, this approach helps optimize the design process, providing alternatives to traditional filters that rely on multiple reactive components for high-order filtering.

Keywords: surface acoustic waves, electronic filters, piezoelectric, numerical simulation.

1. Introduction

Nowadays, sensors are one of the most essential components of any sophisticated electronic system. Their role is indispensable for the functioning of modern electronics. They serve as the interface between the physical world, governed by the laws of physics, and the digital area, which interprets the acquired data for many applications. Thus, sensor technology is emerging in novel application fields and widespread markets such as smart cities, industrial automation and control, communications, and health, among others [1-3].

Once electronic sensors detect and interact with the physical phenomena around them, processing the response data via signals is necessary to comprehend the outcomes once they are analyzed. Then, the measurements can be affected by any background noise source; due to this, the purpose of electronic filters [4] is to eliminate or dim the background noise that could affect the measurements or discriminate a specific frequency that goes through it, allowing the modification of the amplitude and phase [5].

The rate at which something occurs is known as frequency; signals obtained from measurement can be transformed from the time domain to the frequency domain. It has been shown that any waveform that exists in the world can be represented by the addition of multiple sine waves. Amplitudes, frequencies, and phases of these, spliced correctly, can generate a waveform identical to the one desired. Understanding how signals are a combination of multiple waveforms with different amplitudes and frequencies leads to the fact that sometimes, it is necessary to get rid of some of them. A filter is a device that allows just a specified frequency of signals to pass through it, rejecting the ones that do not meet the desired specifications [6].

The frequency response of a circuit is the response when it experiences changes in the input signal frequency. Electronic devices usually have a frequency range where their response is close to the ideal; the output signal can be distorted out of this range. Owing to the device's dependence on the frequency, filters are used to isolate the functional frequencies for the device's optimal operation.

The operating range of each device or circuit depends on the type of components used and their configuration. This determines the cut-off frequency, which is defined as the boundary where the signal passing through the system

begins to be attenuated. There are four basic types of circuit filters based on their behavior near the cutoff frequency.

The low-pass filter allows signals from 0 Hz up to a specified cut-off frequency to pass through, while a high-pass filter only allows high frequencies, typically above 1 kHz. A band-pass filter allows signals within a bandwidth defined by two cut-off frequencies while attenuating those outside it. Conversely, a notch or band-stop filter attenuates waves within a defined range, allowing those outside the limits to pass. Additionally, filters can be classified into two categories passive filters, designed with passive components such as resistors, capacitors, and inductors, or active filters, designed with active components like operational amplifiers [7].

The main complication during the implementation of filters is the real response they have, while operating within the cut-off frequency bandwidth, which is the difference between the higher and lower cut-off frequency, the signal ideally should not exhibit significant distortion in amplitude or phase. An ideal filter should maintain a constant response during the specified period of frequencies and completely remove frequencies higher or lower than the cut-off frequency, depending on the type of filter [8]. However, the real filter output signal gradually decreases or becomes distorted as the frequency approaches the cut-off frequency, making it useless.

Hence, designing filters with a response as close as possible to the ideal response by increasing the filter's order without adding more reactive components (e.g., inductors or capacitors) poses a significant challenge for researchers. Additionally, there is a prevailing trend in the progression of sensor technology towards miniaturization, coupled with a growing utilization of multi-sensor configurations and wireless systems.

Therefore, thanks to advancements in computing and microfabrication techniques, it's now feasible to conceive and fabricate innovative structures tailored for application in sensor technology.

For example, surface acoustic wave (SAW) filters are electromechanical components at the microscale whose operation principle is turning the electrical signals into mechanical waves through the properties of piezoelectric substrates. The operation of this kind of filter begins with the input transducer, which converts the electrical signal to a mechanical wave. This wave propagates across

the surface of the substrate from one end to another. As the wave travels, it interacts with an array of electrodes designed to attenuate or let through the desired frequency. Once the mechanical wave reaches the output transducer, it is converted back to an electrical signal without the undesired frequencies [9].

SAW filters are at the forefront of advancing technologies and high-precision electronic systems. SAW filters are not just limited to one field of high-frequency electronics. Their unique characteristics, such as high selectivity and low insertion loss, make them versatile and ideal for integration into various applications [10]. From wireless communication systems [11] and radars to temperature and pressure sensors and medical devices like heart rate resonators and glucose monitors [12 - 16].

Designing SAW filters involves a process that starts with defining the filter specifications, such as center frequency, bandwidth, and insertion loss requirements. The design typically progresses by selecting appropriate substrate materials with suitable acoustic properties, determining the interdigital transducer (IDT) geometry, and optimizing the electrode configuration for desired performance characteristics. Advanced simulation tools like COMSOL Multiphysics are then utilized to model the SAW filter, analyze its frequency response, and refine the design until meeting the specified criteria.

The application of numerical simulations in COMSOL to design surface acoustic wave (SAW) filters, offers considerable advantages, such as enabling efficient and cost-effective exploration and access to a wide range of design parameters and configurations, which leads to optimized filter performance. Advanced SAW filter simulation of complex physical phenomena by COMSOL significantly aids the comprehension of SAW filter behavior as well as its performance characteristics. This brings the possibility to visualize and analyze simulation results and identify the potential design improvements for fine turning the filter design to meet specific requirements accurately. Implementing COMSOL for SAW filter design ensures a streamlined and efficient design process, resulting in high-performance filters designed especially for each application's needs.

In this work, we present a detailed methodology for the numerical simulation of a surface acoustic wave (SAW) filter using the delay line configuration with lithium niobate in 128° YX LiNbO_3 rotation as a piezoelectric substrate. The methodology covers the conceptualization of filter design as a bandpass filter with

a center frequency at 30 MHz with a Null bandwidth of 3 MHz, the description of the use of COMSOL Multiphysics for numerical simulation divided into the definition of SAW filter's geometry, material properties and boundary conditions, mesh settings, and study configuration. Finally, the results are exported, analyzed, and discussed.

We focused on SAW filter design and simulation due to multiple advantages, such as the miniaturization of electronic filters when compared with LC filters such as Chebyshev, Butterworth, or Bessel filters. For a 3rd order filter, each variation has approximately 3 capacitors and 3 inductors, and the number of components grows proportionally to filter order. Thus, dealing with high numbers of components includes managing with component variation and tolerance properties. By contrast, SAW filters employ the use of a unique electronic passive component made in a single substrate and offer high-temperature stability and precise frequency response.

2. Methodology

2.1. Filter design conceptualization

Different techniques can be used to design surface acoustic wave filters. As a first approach for a bandpass filter design, a delay line configuration was selected, as shown in Figure 1, consisting of two ports of metallic structures deposited on the surface of a piezoelectric substrate with an input port and an output port, each formed by identical interdigital transducers (IDTs) of determined numbers of finger pairs (N_p) with finger width (r), acoustic aperture (W), and separation between ports (l). The IDT geometry and the physical properties of the piezoelectric substrate almost wholly determine the filter's electromechanical behavior.

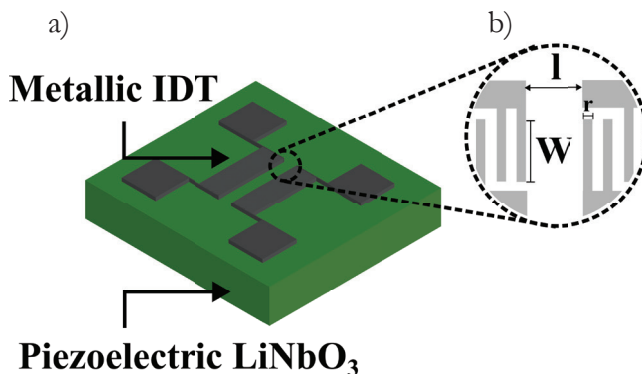


Figure 1. (a) The scheme shows a SAW filter with a delay line configuration. (b) Zooms in on the details of IDT geometry, including the separations between ports (l), acoustic aperture (W), and finger width (r).

COMSOL Multiphysics, like various numerical modeling tools, allows the consistent and straightforward modeling of the filter’s electrical behavior and response to many environmental and microfabrication parameters. However, these numerical simulations in COMSOL were complemented with analytical results to explain the geometrical design of IDTs.

Filter simulation involves precisely defining the geometric parameters and objectives. The operating resonant frequency (f_0), desired performance metrics like Null bandwidth (NBW), the filter’s piezoelectric material selection (the most used materials are Quartz, ZnO, LiTaO₃ or LiNbO₃), and desired ripples level, which in turn defines the insertion loss levels (IL) must be specified.

The most common IDT configurations are single-finger, double-finger, and single-phase unidirectional transducers (SPUDT). Design details of the desired configuration are shown in Table 1 and form the basis for creating an accurate simulation model using COMSOL, ensuring a detailed analysis of the SAW filter’s electrical behavior.

Substrate material	128° YX LiNbO ₃
Electrode configuration	Double finger
Resonant frequency	30 MHz
Null Bandwidth	3 MHz
Phase ripple	<1°
Insertion loss	~-10 dB

Table 1. Principal desired characteristics for the SAW bandpass filter design.

The selection of 128° YX LiNbO₃ as a piezoelectric material is due to its high piezoelectric coupling factor ($k^2= 0.055$), a direct measure of its transduction efficiency. The center frequency is selected for 30 MHz. Still, a similar process is valid for arbitrary frequency, considering that the lower the frequency, the larger the size of the SAW filter, making low-frequency filter fabrication almost impractical. Frequency value is related to IDT geometry through the dispersion relation of Equation 1: $f = v/\lambda$ 1

Where λ is the equivalent acoustic wavelength, the relation between finger width (r) and acoustic wavelength $\lambda = 8r$ is fulfilled for the double-finger IDT configuration. Also, the double-finger geometry is chosen as a non-reflectivity IDT to avoid internal reflection and distortion of frequency response. On the other hand, is the surface acoustic wave velocity propagation, considering the IDT as a dispersive medium given by Equation 2 described by Bløtekjær et al. [17].

$$v = \frac{v_f}{(1 + 0.85(v_f - v_m)/v_m)} \quad 2$$

Where $v_f = 3975$ m/s and $v_m = 3865$ m/s are the free and metalized propagation velocities of SAW in the piezoelectric substrate, respectively.

The frequency response could be represented as a combination of the frequency response of each SAW filter port. We can search desired IL levels and amplitude of phase ripples ($\Delta\alpha$), which are deeply correlated. Usually, we can set the desired levels of amplitude-phase ripples and then relate this with the number of finger pairs through the attenuation of triple transit signals (TTS) and insertion loss, as described by Soluch et al. [18] with

$$2N_p = N^2 \approx \frac{\sqrt{A_{tt} y_1 y_2}}{G_p W/\lambda} \quad 3$$

Where N is defined as the number of spaces between opposite polarity with non-zero overlap, W and λ previously defined, y_1 and y_2 are the source and load admittances and are usually selected as 50Ω , G_p is a constant of conductance dependent on IDT geometry and $A_{tt} \approx \tan(\Delta\alpha)$ is the attenuation of TTS.

For the NBW value,

$$NBW = \frac{2f_0}{N_p} \quad 4$$

Where f_0 is the resonant frequency and N_p is the number of finger pairs.

2.2. Geometry of the SAW filter

All configurations were made to save computational time, taking advantage of available hardware: an Intel core i7 11th Gen. with 32 GB of RAM. We used the piezoelectric branch of the AC/DC module in COMSOL V6.0, which couples electrical and mechanical physics and allows for modeling piezoelectric problems.

The SAW filter was simplified in 2D geometry. The geometry of $N_p = 20$ finger pairs, acoustic aperture $W = 2587.32 \mu\text{m}$, and separation between ports of $l = 1293.6 \mu\text{m}$ were considered for filter design. Figure 2a shows the geometry of an azimuthal cut of the piezoelectric substrate and of the IDT on its surface as shown in Figure 2b, where $w = 16.17 \mu\text{m}$ represents the finger width, $h = 300$ nm the finger thickness, and $\lambda = 129.36 \mu\text{m}$ the equivalent acoustic wavelength.

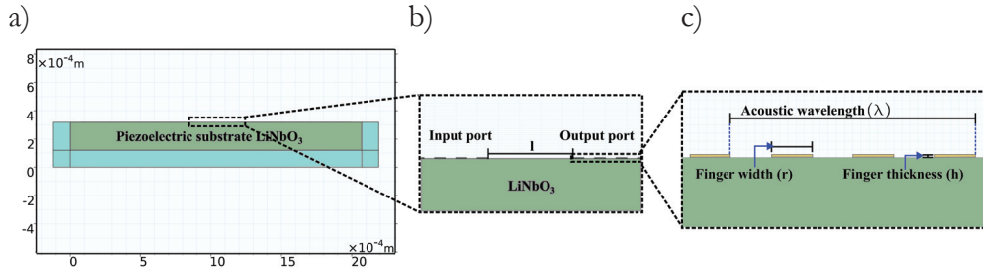


Figure 2. (a) 2D simplification of SAW filter geometry in an azimuthal cut. (b) zoom in on the details of port separation distance (l). (c) Zoom in on the details of the double-finger IDT configuration, including the definition of finger width (r) and finger thickness (h).

2.3. Material properties and boundary conditions

Lithium niobate (LiNbO_3) with a YZ-cut orientation is available in the COMSOL materials library. Obtaining particular cut orientation properties could be done using Euler angles rotation $((0,38,0)$ for 128° YX rotation) or calculating the properties of rotated material as in Auld et al. [19], with the use of rotation matrix operation for piezoelectric constant tensors.

We set the mechanical and electrical boundary conditions once the 128° YX LiNbO_3 properties are defined. Mechanical fixed and free boundary conditions are selected at the bottom and top of the piezoelectric substrate, respectively, as shown in Figure 3a. Equivalent electrical boundary conditions are chosen for the input and output ports, as depicted in Figure 3b, with a selection of ground and terminal boundaries as input excitation sources, such as voltage signals for simulation. Additionally, we use a perfect-matched layer (PML) as a perfectly absorbing domain or nonreflecting boundary condition to avoid reflection of the geometric boundary of the piezoelectric substrate.

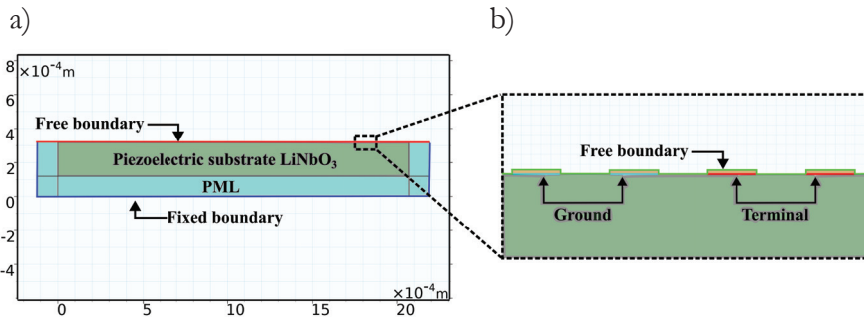


Figure 3. (a) Mechanical boundaries condition with the addition of Perfect Matched Layer (PML). (b) zoom in on the detail of the electrical boundary condition with the definition of excitation condition with ground and terminal configuration

2.4. Study settings

With the aim of optimizing the simulation, we made the necessary configurations from mesh settings. Correctly setting the mesh configuration could reduce the computational time of a frequency-domain study. COMSOL permits the configuration of the mesh geometry as defined by physics or as defined by the user. The second option to enhance the simulation resolution near and directly below the finger geometry was used.

Different configurations permit the use of personalized mesh geometry. The one selected here is the mapped mesh, a particular type of mesh that allows the creation of a quadrilateral mesh for each domain in 2D geometry and maps the mesh to the desired geometry under selected domains to cover any area of interest uniformly.

To create a mapped mesh, we first use a custom element size to control the maximum size. The finger domain and upper boundary to create separate meshes, one controlled by the mesh of the finger's elements and one controlled by the upper edge boundary were selected, as shown in Figure 4a. A distributed mesh along the geometry depth until it reaches the substrate's bottom surface, copying the source mesh to define regular mesh elements at the lower substrate boundary was used (see Figure 4b).

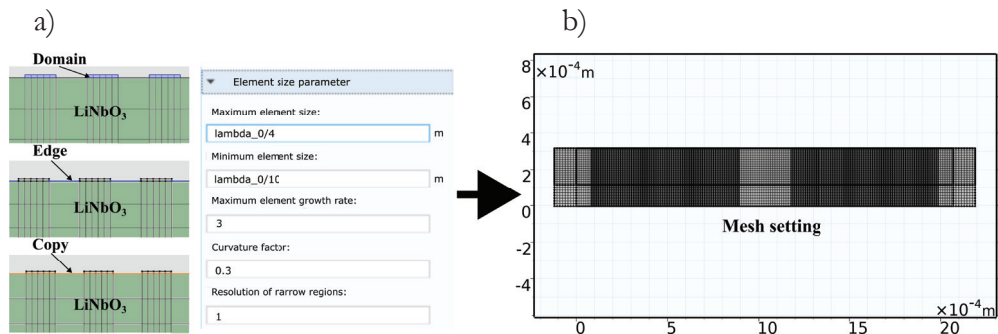


Figure 4. (a) shows the steps to configure a mapped mesh, selecting domains and edges and then copying the mesh properties from one boundary to another, with a desired element size of the quadrilateral mesh. (b) shows the size parameters of the mesh configuration for the mapped mesh geometry.

The filter frequency response is obtained using a frequency domain study configured directly from the main menu and general study selection. For this, it is necessary to set a frequency range with a start, stop, and step value. We use a symmetric frequency interval ranging from $f_0 - 5$ MHz to $f_0 + 5$ MHz with a 0.1 MHz step resolution, see Figure 5a.

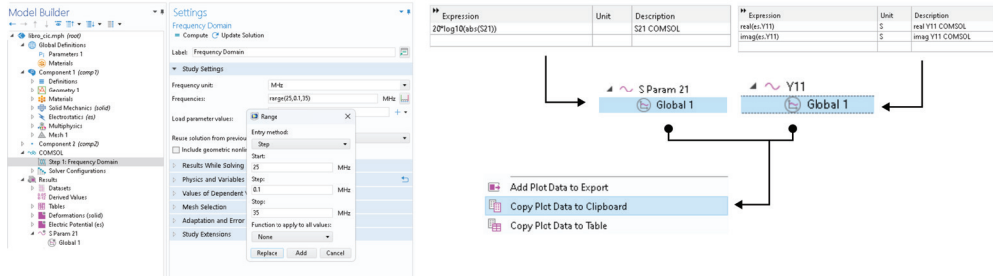


Figure 5. (a) shows the frequency study selection and the definitions of the frequency range. (b) shows the use of S21 for S-parameter definition and es.Y11 special function of COMSOL for Y-parameters in a 1D plot group and its data exportation.

To characterize the filter frequency response through the S_{21} parameter, conductance (G), and susceptance (B), we use a 1D plot group. We obtain the S_{21} parameter using the appropriate COMSOL variable definitions for S-parameters. Using one global subnode of the 1D plot group created, we called the S_{21} variable and operated over this to obtain the IL levels using Equation 5, as shown in Figure 5b:

$$IL = 20 |S_{21}| \quad 5$$

Equivalently, values of conductance (G) and susceptance (B) of each IDT port were extracted, which are related through the relation $Y = G + iB$ for each port. Thus, in another global subnode, we use the COMSOL definition of Y-parameters; we call the $es.Y11$ variable as $real(es.Y11)$ to obtain the real part of admittance (conductance) and $imag(es.Y11)$ to get the imaginary part of admittance (susceptance).

Once obtained, the results could be exported to plot externally in any graphical analysis software by copying the data, clicking right on the global subnode, and selecting the option of copying plot data to the clipboard (see also Figure 5b).

3. Results and discussion

Once exported, the simulation data was plotted using OriginPro software. As shown in Figure 6a, the frequency response of a SAW filter with IL levels at the resonant frequency of -10.39 dB, Null Bandwidth of 3 MHz, and average side lobe levels of $SLL = -33.01$ dB, all near the desired characteristics of the SAW filter is shown. On the other side, Figure 6b shows the conductance and

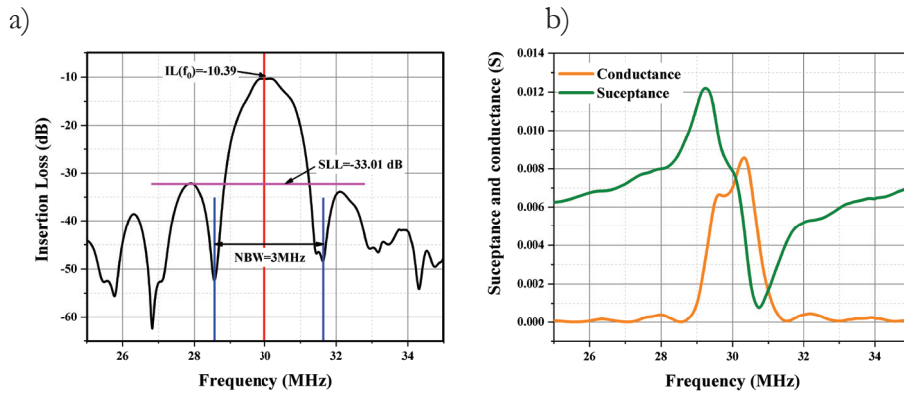


Figure 6. (a) shows the frequency response of the SAW filter, showing the insertion loss at the resonant frequency, side lobe levels, and Null bandwidth value, and (b) Graph shows the conductance and susceptance response.

susceptance results, easily extracted from simulation, showing a maximum conductance value of 83 mS and maximum and minimum values of susceptance of 120 mS and 8 mS, respectively.

While the frequency response obtained corresponds with the classical band-pass filter response, and its characteristics represent part of the electrical behavior of the filter SAW, the conductance and susceptance response complement crucial information about filter behavior. As a designer, is important to consider the frequency response distortion caused by undesired effects of mass loading due to the deposition of the metallic structure that conforms to the IDT geometry, generation of triple transit signals (TTS), bulk wave generation, etc., some of this distortion effects could be avoided analyzing the conductance and susceptance behavior. Susceptance and conductance response symmetry is expected when distortion is nullified. For example, much of the distortion or frequency shift of maximum conductance value to higher or lower values could be attributed to second-order effects.

More than frequency response or susceptance and conductance values, COMSOL enables other special functions that could be called with simple line commands. For example, we can extract the deformation measurement from Rayleigh surface displacement, as shown in Figure 7a, using u , v , or w field displacement in a 2D plot group. Similarly, we can use the voltage variable V in a 2D plot group to plot the electric potential distribution, as shown in Figure 7b. Both functions could perform different analyses of wave travel and potential distribution as a function of waveguides deposited on filter surfaces or temperature compensation of SAW filters.

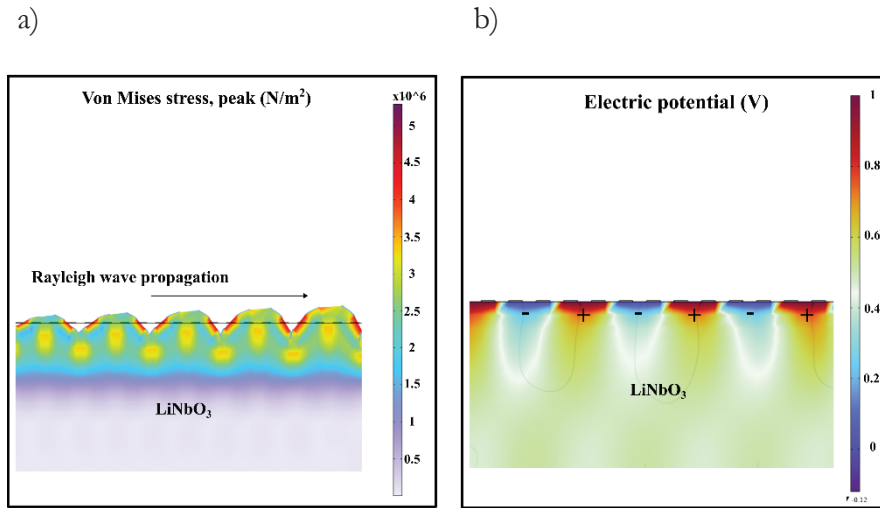


Figure 7. (a) Surface deformation of piezoelectric substrate. (b) Electric potential travels in the volume of LiNbO₃, where the distribution of electric potential is depicted graphically.

The presented work includes the analysis of key factors suitable for an SAW filter design such as its frequency response, conductance, susceptance, substrate deformation, and the electric potential distribution. Using computational tools like COMSOL allows engineers and researchers to obtain a deep understanding of the physical mechanisms influencing the behavior of these filters. These tools have wide advantages compared to analytical methods, such as more precise tuning and enhanced filter response. Furthermore, the use of numerical simulations reduces the time used in the design process and opens the door to advanced design techniques when combined with machine learning and artificial intelligence tools.

4. Conclusions

We presented a 2D numerical simulation methodology of a SAW bandpass filter design using the COMSOL Multiphysics software. The methodology permits to analyze and simulate the scattering parameters, conductance, and susceptance values as well as the 2D visualization of the voltage propagation and the material surface deformation, usable to measure the acoustic surface energy. The methodology includes the definition of piezoelectric properties, geometric configurations, and the necessary boundary conditions to replicate the electromechanical behavior of the device.

The numerical results showed insertion loss levels of $IL = -10.39$ dB, $SLL = -33.01$ dB, and $NBW = 3$ MHz. These values permit effectively obtaining a bandpass filter with the levels of phase ripples imposed sacrificing the increase in the IL to the levels shown. On the other side, the simulations reveal conductance maximum values of 83 mS, and susceptance measurements presented maximum and minimal values of 120 mS and 8 mS, respectively. Furthermore, the use of numerical simulation tools permits to enhancement of the study of physical mechanisms including the voltage SAW propagation and surface deformation of piezoelectric material, something that opens the door to advanced design techniques including waveguiding.

All the calculations were made using 2D COMSOL simplification, to save time and computational costs, simulations were made with 0.1 MHz steps, and computed within 20 minutes. The satisfactory results validate, prove, and promote COMSOL Multiphysics for SAW filter design. Thus, this methodology achieves specific goals: firstly, it acts as a comprehensive guide for new students and researchers in the development of numerical simulations, and secondly, it generates a broad and deep understanding of the complex electromechanical behavior of SAW filters. These filters are widely acknowledged as an alternative to conventional filter design techniques.

Acknowledgments

The authors would like to thank the Instituto Politécnico Nacional for the use of its facilities, the BEIFI SIP20241279, SIP20240477, and SIP20241266 projects, and CONAHCYT for its support with postgraduate scholarships and the project CONAHCYT N°319037 “Escuela Mexicana de Ventilación”.

References

1. Park, J., Kim, K. T., & Lee, W. H. (2020). Recent advances in information and communications technology (ICT) and sensor technology for monitoring water quality. *Water (Switzerland)*, 12(2).
<https://doi.org/10.3390/w12020510>
2. Guerrero-Ibáñez, J., Zeadally, S., & Contreras-Castillo, J. (2018). Sensor technologies for intelligent transportation systems. *Sensors (Switzerland)*, 18(4).
<https://doi.org/10.3390/s18041212>
3. Morello, R., Mukhopadhyay, S. C., Liu, Z., Slomovitz, D., & Samantaray, S. R. (2017). Advances on sensing technologies for smart cities and power grids: A review. *IEEE Sensors Journal*, 17(23).
<https://doi.org/10.1109/JSEN.2017.2735539>
4. Singh, B., AlHaddad, K., & Chandra, A. (1999). A review of active filters for power quality improvement. *IEEE Transactions on Industrial Electronics*, 46(5).
<https://doi.org/10.1109/41.793345>
5. Sáenz, E. M., de la Cruz, J. P., & Garzón, H. S. (2020). *Fundamentos de circuitos eléctricos II*.
6. Williams, A. B., & Taylor, F. J. (2006). *Electronic filter design handbook, Fourth Edition. Proceedings of the IEEE*, 70(3).
7. Dimopoulos, H. G. (2012). *Analog electronic filters: Theory, design and synthesis*.
<https://doi.org/10.1007/978-94-007-2190-6>
8. Chen, P., Li, G., & Zhu, Z. (2022). Development and application of SAW filter. *Micromachines*, 13(5).
<https://doi.org/10.3390/mi13050656>
9. Morgan, D., & Paige, E. G. S. (2007). *Surface acoustic wave filters: With applications to electronic communications and signal processing*.
10. Mandal, D., & Banerjee, S. (2022). Surface acoustic wave (SAW) sensors: Physics, materials, and applications. *Sensors*, 22(3).
<https://doi.org/10.3390/s22030820>
11. Pan, Y., Mu, N., Liu, B., Cao, B., Wang, W., & Yang, L. (2018). A novel surface acoustic wave sensor array based on wireless communication network. *Sensors (Switzerland)*, 18(9).
<https://doi.org/10.3390/s18092977>
12. Luo, J., et al. (2013). A new type of glucose biosensor based on surface acoustic wave resonator using Mn-doped ZnO multilayer structure. *Biosensors and Bioelectronics*, 49.
<https://doi.org/10.1016/j.bios.2013.05.021>

13. Agostini, M., Greco, G., & Cecchini, M. (2019). Full-SAW microfluidics-based lab-on-a-chip for biosensing. *IEEE Access*, 7.
<https://doi.org/10.1109/ACCESS.2019.2919000>
14. Liu, B., et al. (2016). Surface acoustic wave devices for sensor applications. *Journal of Semiconductors*, 37(2).
<https://doi.org/10.1088/1674-4926/37/2/021001>
15. Liu, X., Chen, X., Yang, Z., Xia, H., Zhang, C., & Wei, X. (2023). Surface acoustic wave-based microfluidic devices for biological applications. *Sensors and Diagnostics*, 2(3).
<https://doi.org/10.1039/D2SD00203E>
16. Länge, K., Rapp, B. E., & Rapp, M. (2008). Surface acoustic wave biosensors: A review. *Analytical and Bioanalytical Chemistry*.
<https://doi.org/10.1007/s00216-008-1911-5>
17. Bløtekjær, K., Ingebrigtsen, K. A., & Skeie, H. (1973). Acoustic surface waves in piezoelectric materials with periodic metal strips on the surface. *IEEE Transactions on Electron Devices*, 20(12).
<https://doi.org/10.1109/T-ED.1973.17807>
18. Soluch, W. (1998). Design of SAW delay lines for sensors. *Sensors and Actuators A: Physical*, 67(1–3).
[https://doi.org/10.1016/S0924-4247\(97\)01737-8](https://doi.org/10.1016/S0924-4247(97)01737-8)
19. Auld, B. A., & Green, R. E. (1974). Acoustic fields and waves in solids: Two volumes. *Physics Today*, 27(10).
<https://doi.org/10.1063/1.3128926>